

In Vivo Neuroimaging of Exosomes Using Gold Nanoparticles

Oshra Betzer,^{†,‡,⊥} Nisim Perets,^{§,⊥} Ariel Angel,[§] Menachem Motiei,[†] Tamar Sadan,[†] Gal Yadid,^{‡,⊥} Daniel Offen,[§] and Rachela Popovtzer^{*,†}

[†]Faculty of Engineering and the Institute of Nanotechnology & Advanced Materials, [‡]The Leslie and Susan Gonda Multidisciplinary Brain Research Center, and [⊥]Everard and Mina Goodman Faculty of Life Sciences, Bar-Ilan University, Ramat Gan, 5290002, Israel

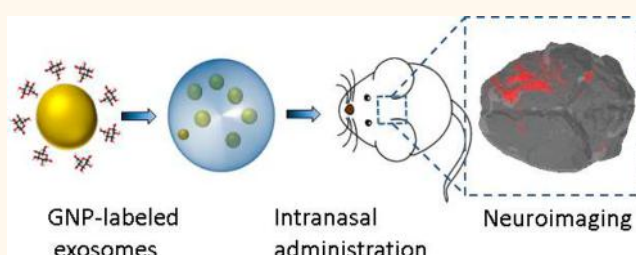
[§]Felsenstein Medical Research Center, Sackler Faculty of Medicine, Tel Aviv University, Tel Aviv 69978, Israel

Supporting Information

ABSTRACT: Exosomes are emerging as effective therapeutic tools for various pathologies. These extracellular vesicles can bypass biological barriers, including the blood-brain barrier, and can serve as powerful drug and gene therapy transporters. However, the progress of therapy development is impeded by several challenges, including insufficient data on exosome trafficking and biodistribution and the difficulty to image deep brain structures *in vivo*. Herein, we established a method for noninvasive *in vivo*

neuroimaging and tracking of exosomes, based on glucose-coated gold nanoparticle (GNP) labeling and computed tomography imaging. Labeling of exosomes with the GNPs was achieved directly, as opposed to the typical and less efficient indirect labeling mode through parent cells. On the mechanistic level, we found that the glucose-coated GNPs were uptaken into MSC-derived exosomes *via* an active, energy-dependent mechanism that is mediated by the glucose transporter GLUT-1 and involves endocytic proteins. Next, we determined optimal parameters of size and administration route; we demonstrated that 5 nm GNPs enabled improved exosome labeling and that intranasal, compared to intravenous, administration led to superior brain accumulation and thus enhanced *in vivo* neuroimaging. Furthermore, using a mouse model of focal brain ischemia, we noninvasively tracked intranasally administered GNP-labeled exosomes, which showed increased accumulation at the lesion site over 24 h, as compared to nonspecific migration and clearance from control brains over the same period. Thus, this exosome labeling technique can serve as a powerful diagnostic tool for various brain disorders and could potentially enhance exosome-based treatments for neuronal recovery.

KEYWORDS: neuroimaging, exosomes, gold nanoparticles, computed tomography, brain ischemia



Exosomes are emerging as an effective therapeutic tool for various pathologies, which cannot be treated by conventional medicine. These sub-micron-sized vesicles are secreted by different cell types and participate in intercellular communication by fusing with the recipient cell membrane and thus delivering their payload (genetic information and proteins) to the cell.¹ Therefore, exosomes can serve as powerful drug and gene therapy transporters.^{2–7} In particular, exosomes derived from mesenchymal stem cells (MSCs) exhibit functionality that is similar to parent MSCs, including targeting and decreasing inflammation, repairing tissue damage, and modulating the immune system.^{6,8–11} Thus, MSC-derived exosomes can provide beneficial effects parallel to MSC-based therapy,^{8,12,13} while avoiding the many risks associated with MSC transplantation. Moreover, exosomes possess an intrinsic ability to cross biological barriers, enabling them to bypass the blood-brain barrier (BBB) and transport their payload into the brain.^{14–18} Therefore, an exosome-based,

cell-free therapy has the potential to provide treatments for various diseases and especially for brain pathologies.

However, various issues need to be elucidated before MSC-derived exosomes can be used as therapeutics, including trafficking and communication mechanisms and *in vivo* biodistribution and pharmacokinetics of exogenously administered exosomes.¹⁹ Imaging modalities can provide important information on these issues. Recent studies have demonstrated the ability to image exosomes within the body, mainly using various optical modalities and mostly for cancer research.^{5,9,20} Yet the most common fluorescent and optical imaging modalities have limited ability to image exosomes within deep brain structures.^{21–23}

Herein, we demonstrate a method for noninvasive *in vivo* computed tomography (CT) imaging and tracking of MSC-

Received: June 27, 2017

Accepted: September 29, 2017

Published: September 29, 2017

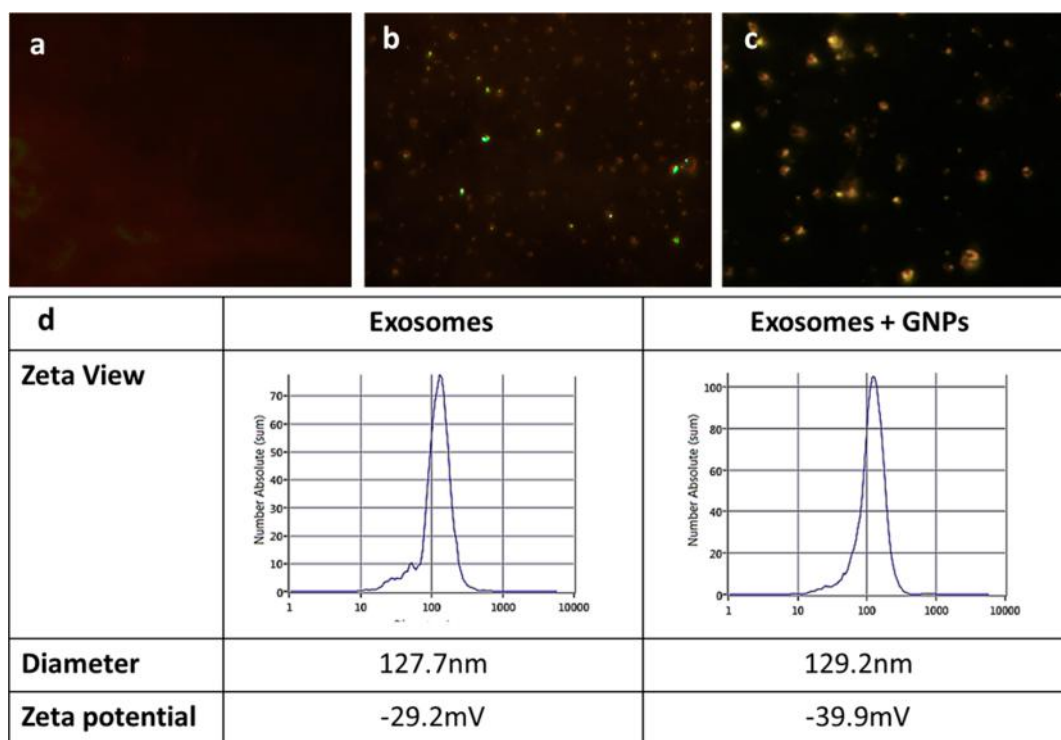


Figure 1. Efficiency of exosome labeling. (a–c) Dark-field microscope (40 \times) images of exosomes: (a) without GNPs; (b) labeled with 5 nm GNPs; and (c) labeled with 20 nm GNPs. (d) ZetaView measurements of mean hydrodynamic diameter and ζ -potential of free exosomes and 5 nm GNP-labeled exosomes obtained at room temperature and at a scattering angle of 90 $^\circ$.

derived exosomes within the brain, by direct labeling with gold nanoparticles (GNPs). For labeling and neuroimaging of the exosomes, we established a protocol that is based on our previous studies,^{10,24–29} demonstrating that GNPs are ideal contrast agents for *in vivo* CT imaging and cell tracking.^{30–32} Typically, an inefficient and indirect exosome labeling approach is used, wherein contrast agents or other substances are introduced into parent cell cultures and uptaken by endocytic pathways; secreted exosomes are then collected from the extracellular environment.^{5,12,17} This indirect approach results in only a small fraction of GNPs within exosomes.^{33,34} Therefore, herein, we applied direct labeling of the exosomes with GNPs, which was found to be efficient and further revealed important components of the GNP uptake mechanism. Moreover, we established optimal labeling and neuroimaging parameters by examining different GNP sizes and exosome administration routes. As recent studies have shown that MSC-derived exosomes promote neuronal and functional recovery,^{35–37} we additionally examined our technique in an ischemic stroke mouse model. Our method enabled non-invasive tracking of intranasally administered GNP-labeled exosomes, which showed higher brain accumulation and prolonged presence at the lesion area, up to 24 h.

RESULTS AND DISCUSSION

Glucose-Coated GNPs and Exosome Preparation. To find the optimal GNP size for the exosome labeling protocol, GNPs sized 5 and 20 nm were synthesized and characterized. The particles were covalently coated with glucose to facilitate uptake of the particles by exosomes (Supporting Information Figures S1–S3), based on a recently published protocol.^{26,38}

Exosomes were purified from human MSCs as previously described³⁹ and evaluated for amount, concentration, and size distribution (Supplementary Figure S4).

Exosomes Are Directly Labeled with Glucose-Coated GNPs. First, we examined the feasibility of GNP uptake by the exosomes. As the exosomal membrane reflects the topology and structural features of the parent cell membrane,^{40–42} we hypothesized that it would be possible to label the exosomes directly and not indirectly through parent cell mechanisms.

Exosomes (2.8×10^{10}) were incubated with 5 and 20 nm glucose-coated GNPs for 3 h at 37 $^\circ\text{C}$ and then centrifuged and washed. The efficiency and viability of exosome labeling was confirmed by dark-field microscopy images, dynamic size, and ζ -potential measurements (Figure 1). Dark-field images distinctly demonstrated GNP uptake into exosomes (Figure 1a–c). The diameter of the exosomes containing GNPs was not altered as compared to nonlabeled exosomes, though the ζ -potential became slightly more negative, possibly due to negative nanoparticles still attached to the exosome surface (Figure 1d).

Exosomes Exhibit an Active Uptake Mechanism of Glucose-Coated GNPs. As the exosomes were labeled directly, and not through parent cells, we next investigated the mechanism underlying this phenomenon in a series of experiments. Two different GNP sizes (5 and 20 nm) were examined, as nanoparticle size plays a role in cell and exosome internalization.^{20,43}

GNP Internalization Is Energy-Dependent. First, we examined whether internalization of the particles into exosomes is primarily energy-dependent or, alternatively, occurs through membrane diffusion. Exosomes (total of 2.8×10^{10} here and in experiments below) were incubated for 3 h with glucose-coated GNPs (35 mg/mL; here and below) at 37 or 4 $^\circ\text{C}$. Flame

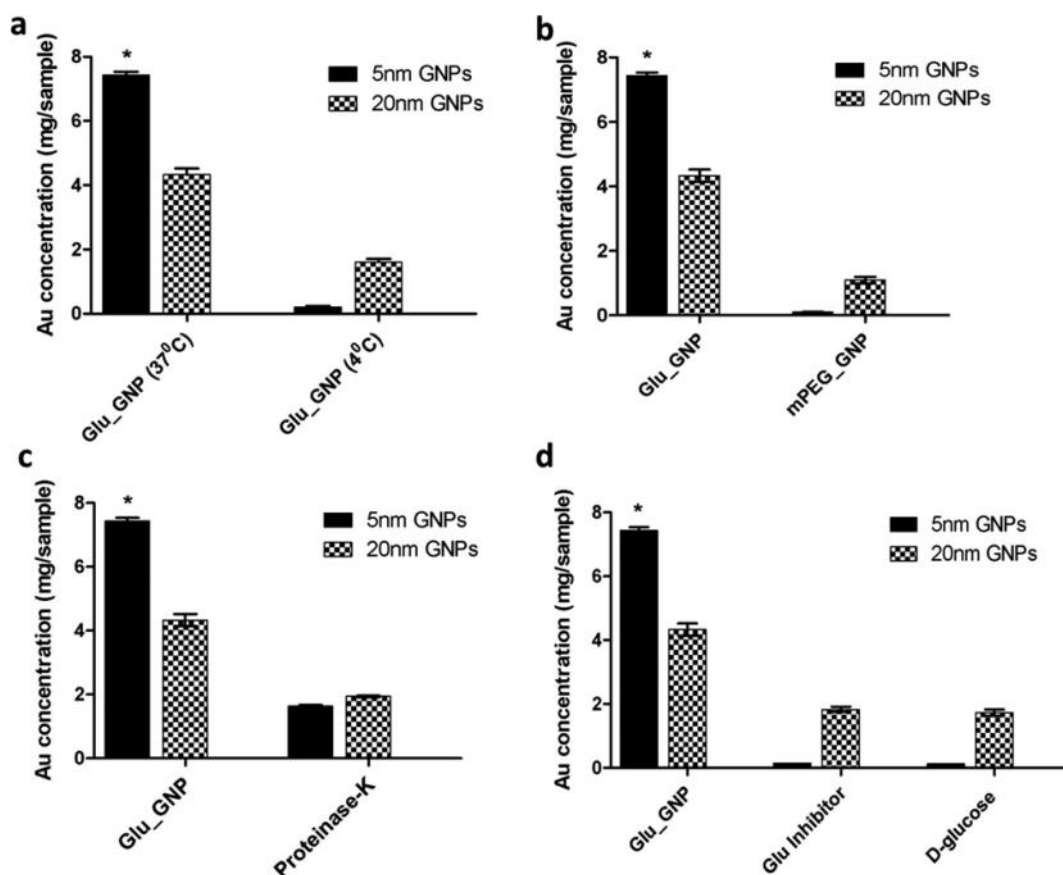


Figure 2. Characterization of exosome uptake of GNPs. FAAS quantification of GNPs sized 5 and 20 nm after 1 h incubation with exosomes under different conditions. (a) Temperature = 4 or 37 °C. (b) Glucose coating: glucose-coated GNPs (Glu_GNP) and control GNPs without glucose (coated with mPEG). (c) Modifying exosomal membrane: proteinase-K treatment given prior to particle loading. (d) Glucose inhibition and saturation: treatment with cytochalasin B, a glucose transport inhibitor, or saturation of D-glucose in medium. Significant differences were detected in gold concentrations within the exosomes between glucose-coated nanoparticles of both sizes (at 37 °C) and all other conditions ($p < 0.001$; Student's t test), verifying that the uptake into the exosomes occurred through an active mechanism, mediated by GLUT-1.

atomic absorption spectroscopy (FAAS) measurements revealed a clear and significant reduction in uptake at 4 °C as compared to 37 °C for both sizes ($p < 0.001$; Student's t test), yet this decrease was especially dramatic for 5 nm GNPs (Figure 2a). This finding implies that GNPs are internalized by exosomes mainly through active, energy-dependent uptake and not membrane diffusion. This result is consistent with the literature on cellular uptake of nanoparticles, showing that this process is mediated through energy-dependent, temperature-sensitive endocytosis.^{44–47}

GNP Uptake Is Primarily Attributable to Its Glucose Coating. Next, we examined whether the uptake of GNPs can be attributed their to glucose coating. Exosomes were incubated (3 h, 37 °C) with either glucose-coated GNPs or control GNPs with an mPEG linker and no glucose coating (5 or 20 nm, for both types). FAAS analysis showed a clear reduction in particle uptake for both sizes of noncoated GNPs as compared to glucose-coated GNPs. It is notable that 5 nm GNP size also showed enhanced internalization with glucose coating compared to that with the corresponding 20 nm GNPs ($p < 0.001$, Figure 2b).

Exosome Membrane Proteins Play a Role in Active Uptake of GNPs. To study a possible role for exosome membrane proteins in GNP uptake, we used proteinase-K (proK), a nonspecific serine endopeptidase which destructs proteins in

their native states.⁴⁸ Exosomes were incubated with proK (10 min, 55 °C), followed by incubation with proteinase-K inhibitor (7 min) and GNPs (3 h, 37 °C). We found a significantly lower uptake level of both GNP sizes in pro-K-treated as compared to nontreated exosomes (over 80% reduction for 5 nm GNPs; $p < 0.001$), indicating the involvement of exosome membrane proteins in active uptake pathways of the glucose-coated GNPs (Figure 2c).

Uptake Is Associated with GLUT-1 Glucose Transporter.

We next endeavored to find a specific membrane protein that may be involved in the active uptake process. We hypothesized that the glucose coating of the GNPs may lead to their uptake by a glucose transporter. As cellular uptake of glucose and glucose-coated particles is attributed to the glucose transporter GLUT-1,^{49,50} we examined whether the exosome uptake mechanism involves GLUT-1, as well. Exosomes were co-incubated (3 h, 37 °C) with glucose-coated GNPs and with high concentrations of free glucose, which occupies and saturates GLUT-1 at the exosome surface,^{51,52} or with cytochalasin B (CB), a well-known GLUT-1 inhibitor.⁵³ As demonstrated by FAAS analysis, saturation of the medium with high free glucose levels significantly inhibited the uptake of 20 nm GNPs and even more so of 5 nm GNPs, as compared to the uptake achieved at lower glucose levels in the standard medium ($p < 0.001$). Similarly, preincubating exosomes with CB

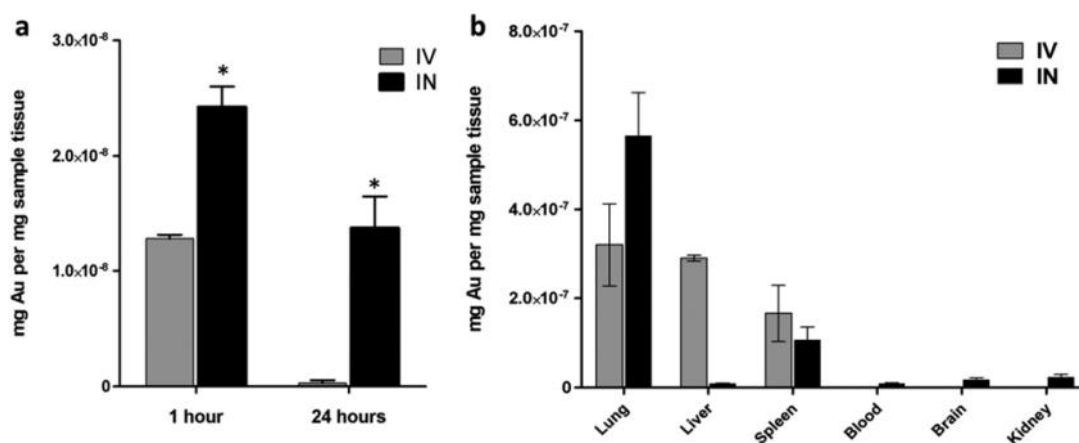


Figure 3. Exosome biodistribution. (a) FAAS quantification of gold within the brain, 1 and 24 h post-IV or post-IN injection. IN administration showed significantly higher gold amounts than IV administration at both time points ($p < 0.01$). (b) FAAS quantification of gold 24 h post-IV or post-IN injection of GNP-labeled exosomes.

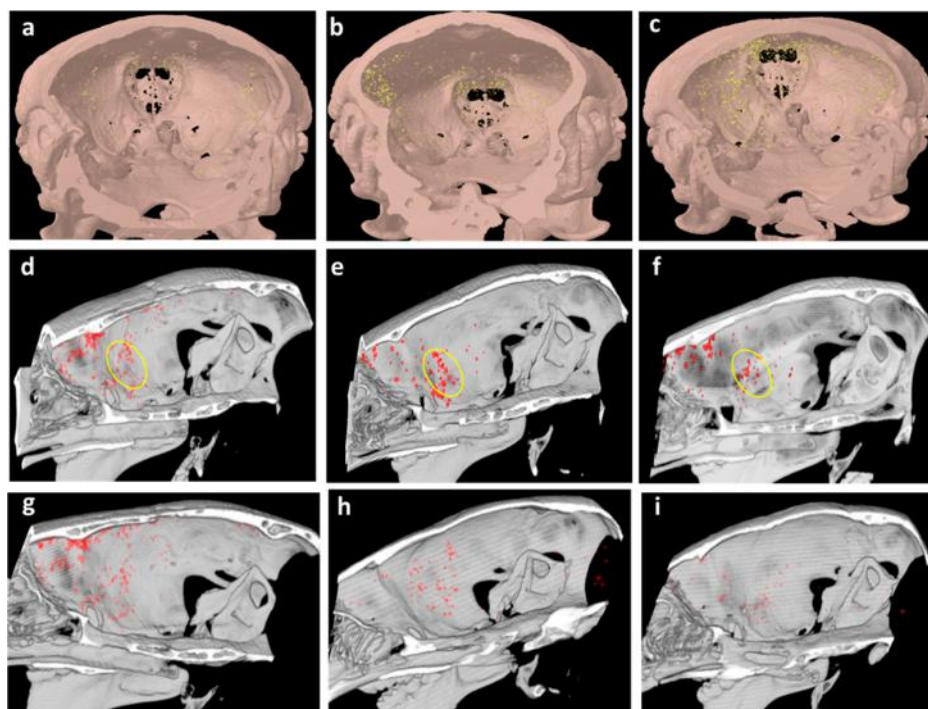


Figure 4. *In vivo* CT imaging of exosomes after acute striatal stroke in a mouse model. (a–f) Ischemic brain: coronal and sagittal three-dimensional (3D) volume rendering views of representative brain, wherein ischemic insult was induced in the striatum in the right hemisphere: (a,d) 1 h, (b,e) 3 h, and (c,f) 24 h post-exosome administration (the ischemic region is demarcated in yellow circle). Exosomes can be seen to migrate and accumulate at the ischemic region at 3 h. (g–i) Control brain: sagittal 3D volume rendering views of control mouse brain: (g) 1 h, (h) 3 h, and (i) 24 h post-exosome administration. Exosomes penetrated the brain but did not specifically accumulate in any region and were cleared from the brain over 24 h post-administration.

significantly inhibited the cellular uptake level of both GNP sizes ($p < 0.001$) (Figure 2d).

Taken together, the above results suggest that glucose-coated nanoparticles are loaded into exosomes *via* an active, energy-dependent mechanism that is mediated by GLUT-1. For the subsequent *in vivo* tests, 5 nm glucose-coated GNPs were used, as exosome uptake of this size was significantly higher than 20 nm under all conditions ($p < 0.001$, Student's *t* test).

Intranasal Administration Leads to Superior Brain Accumulation of GNP Exosomes. We next examined brain accumulation and whole-body biodistribution of the GNP-labeled exosomes after IV (intravenous) and IN (intranasal)

administration. IN drug delivery is emerging as a promising and efficient therapeutic strategy for noninvasive treatment of various CNS diseases. The nasal cavity offers the potential for rapid systemic drug absorption at greatly enhanced concentrations and rapid onset of action, circumventing the obstacles of the BBB.^{54,55} Moreover, noninvasive therapy is desirable particularly for patients with diseases that require chronic dosing.⁵⁶

GNP-labeled exosomes (2.8×10^9) were injected either IV or IN into C57 mice; organs were collected 24 h later, and the gold amount was quantified by inductively coupled plasma (ICP) spectrometry. Within the brain, we found that the

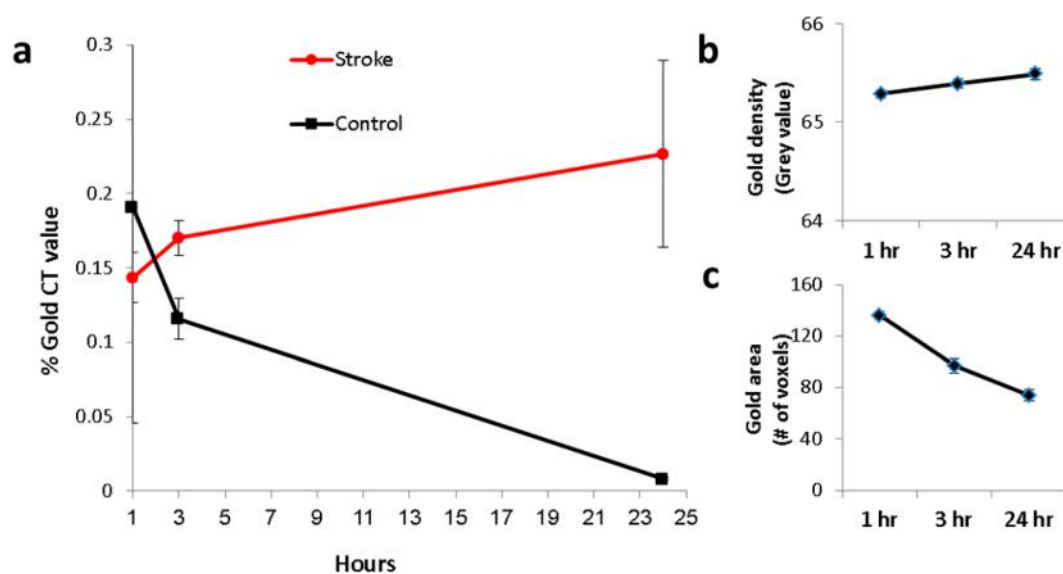


Figure 5. *In vivo* CT analysis of exosomes in stroke area. (a) Measurements of contrast enhancement in whole brain and in the ischemic striatum over time. A gradual increase in CT signal was observed in the ischemic area over 24 h, while the signal decreased over time in control mice. ROI analysis: (b) gold density in the stroke region shows a slight increase, as measured by gray values scale within the ischemic area, and (c) gold area shows a slight decrease, as shown by the number of voxels containing gold within the ischemic area.

amount of exosomes was significantly greater ($p < 0.001$) 1 h after IN administration as compared to 1 h after IV administration (Figure 3a). Twenty-four hours post-administration, a lower, yet nonetheless substantial, amount of exosomes was seen after IN administration, whereas a negligible amount was seen after IV administration, indicating longer intrabrain duration for the IN mode and more rapid clearance of the exosomes from the brain for the IV mode.

Whole-body biodistribution was also evaluated (Figure 3b), and as expected, the route of administration affected exosome distribution and clearance. A significant difference in liver accumulation was found between the two administration modes after 24 h; this result is in accordance with a previous study, which showed that IV injection resulted in higher accumulation within the liver.⁵⁷

These results indicate that following IN administration, exosomes show more widespread biodistribution and, in particular, demonstrate enhanced brain accumulation over a longer period. These findings are supported by other research which used *ex vivo* confocal imaging to show higher catalase-loaded exosome accumulation in brain following IN administration.¹⁷ As the IN mode leads to improved brain accrual and is less invasive, we used this route for delivery of GNP-labeled exosomes in the subsequent *in vivo* experiments.

In Vivo CT Imaging Reveals Selective Accumulation of Exosomes within Stroke Region. The ability to image and track exosomes *in vivo* remains a key challenge for developing exosome-based therapies. Deep brain tissue poses an even greater challenge for *in vivo* imaging, due to the skull barrier that blocks optical signals.^{43,58} Therefore, we next examined whether the exosomes can be noninvasively imaged within the brain, using GNP labeling and computed tomography. We assessed this in an animal model of stroke, as MSC-derived exosomes have been previously shown to promote neuronal and functional recovery in this pathology.^{35–37,59} C57bl/6 male mice received a single, unilateral intrastratial injection of either the vasoconstrictor endothelin-1, to induce focal ischemic-like damage, or saline as control ($n = 3$ for both groups). One day

later, labeled exosomes (2.8×10^9) were administered IN to all mice. *In vivo* CT scans were conducted at 1, 3, and 24 h post-exosome administration. These time points were chosen because the amount of gold that enters the brain *via* the exosomes is relatively small, and thus in some cases, it is more challenging to detect small differences between consecutive scans or visualize real-time migration.

Exosomes were detected within the brain as early as 1 h post-IN administration, in both endothelin-1-treated and saline-treated controls (Figure 4). Migration and accumulation of exosomes at the endothelin-1 injection area in the striatum were seen at 3 h (Figure 4e). After 24 h, exosomes were still detected within the stroke area at a similar amount (Figure 4c,f). In control mice, the exosomes did not show region-specific accumulation and cleared from the brain over the 24 h period.

Contrast enhancement within the brain over time was further noninvasively quantified by region of interest (ROI) analysis (Figure 5a). As a measure of CT intensity, the percentage of gold voxels (voxels with high differential density) within the brain ROI was calculated. Gold voxels were determined based on a minimum gray value threshold, which was defined to be higher than the grayscale indices in the brain before exosome administration. These measurements further verified that, within damaged brains, the gold value—denoting the amount of exosomes—increased over 24 h after IN administration, whereas the control group demonstrated an opposite trend, that is, a decrease in gold value over the same period (Figure 5a). We further calculated the gold volume within the ischemic striatum (number of voxels containing gold) and the average density within these voxels over time. We found that the gold volume of the exosomes per area decreased, while the average density slightly increased (Figure 5b,c), verifying the accumulation of the exosomes within the ischemic region over the experimental period.

Quantifying Exosomes and Verifying Brain Location Using Ex Vivo Imaging. Twenty four hours post-administration, we further verified the location and quantified the

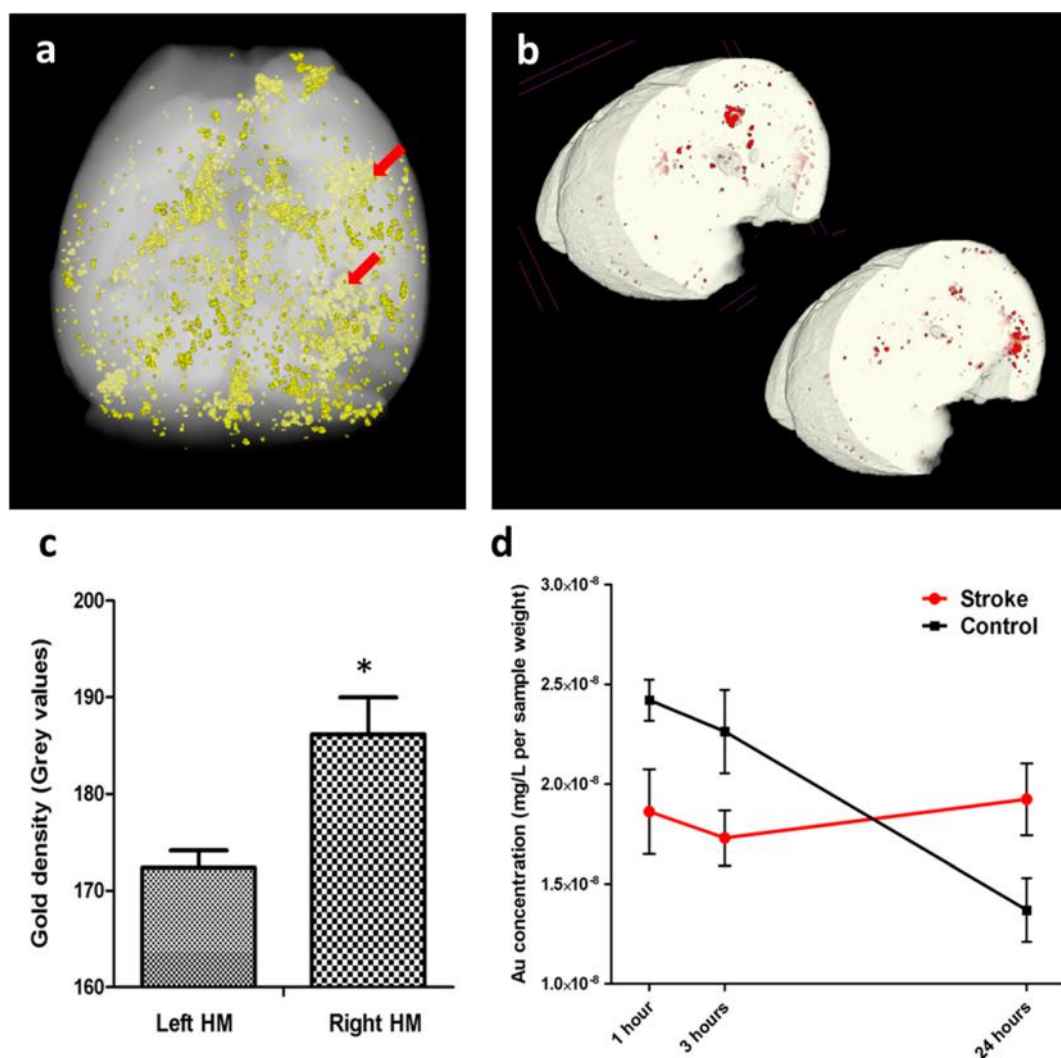


Figure 6. *Ex vivo* imaging and gold quantification within the brain: (a) 3D volume rendering of brain 24 h post-IN administration of GNP-labeled exosomes (exosomes seen in yellow, red arrows point to stroke area). (b) Representative 3D CT-Vox images of two brain sections in the vicinity of the stroke area (striatum). The exosomes are colored in red. (c) CT analysis of gold density within the right hemisphere as compared to the left hemisphere of the ischemic brain. Gold density is significantly higher in the ischemic right hemisphere ($p < 0.05$). (d) ICP analysis of gold within ischemic and control brains, 1, 3, and 24 h post-IN administration of GNP-labeled exosomes.

amount of exosomes within the ischemic brain *ex vivo*, based on the GNP labeling and using higher resolution and radiation dose.

A three-dimensional *ex vivo* image demonstrates the accumulation of exosomes within the brain (Figure 6a,b). Further analysis showed that exosomes were scattered over the brain, and in particular, a large amount accumulated at the stroke region in the right hemisphere, as compared to the same region in the left hemisphere. CT analysis showed that the gold density in the ischemic right hemisphere was significantly higher compared to that in the left hemisphere ($p < 0.05$) (Figure 6c). Additionally, ICP analysis showed that the gold density within the stroke region (right striatum) was significantly higher than that in the rest of the brain ($p < 0.01$) (Supplementary Figure S5). Based on ICP quantification of the gold amount and on the Nanosight assessment of the number of exosomes in the administered dose, we estimated that an amount of $\sim 1.37 \times 10^6$ exosomes reached the stroke area.

Next, we compared between gold concentrations in the ischemic and control (nonischemic) brains, using *ex vivo*

quantitative ICP analysis at 1, 3, and 24 h after GNP-labeled exosome administration. We revealed that a substantial amount of gold reached the ischemic brain and was maintained at a similar level over 24 h, while a steady decline in total gold amount was detected in control brains over this period (Figure 6d). Using the same methods as above, the number of exosomes was estimated to be 7.02×10^7 within the ischemic brain and only 3.12×10^3 within the nonischemic brain. We hypothesize that the reason for this difference is that the exosomes, which are MSC-derived, inherit their parent cell capabilities of homing to, and persisting within, injury areas.^{8,59,60}

We further examined whether the GNPs remain within the exosomes during the 24 h of experiment. Free GNPs (5 nm) were injected (IN, $n = 3$ ischemic mice), and CT scanning was conducted at several intervals, up to 24 h. After 1 h, only few particles are seen in the nasal region and not within the brain; after 24 h, no particles were detected by CT, neither in the nasal region nor within the brain (Supplementary Figure S6a,b). ICP quantification of the whole brain confirmed these results, showing that after 24 h the amount of free GNPs was

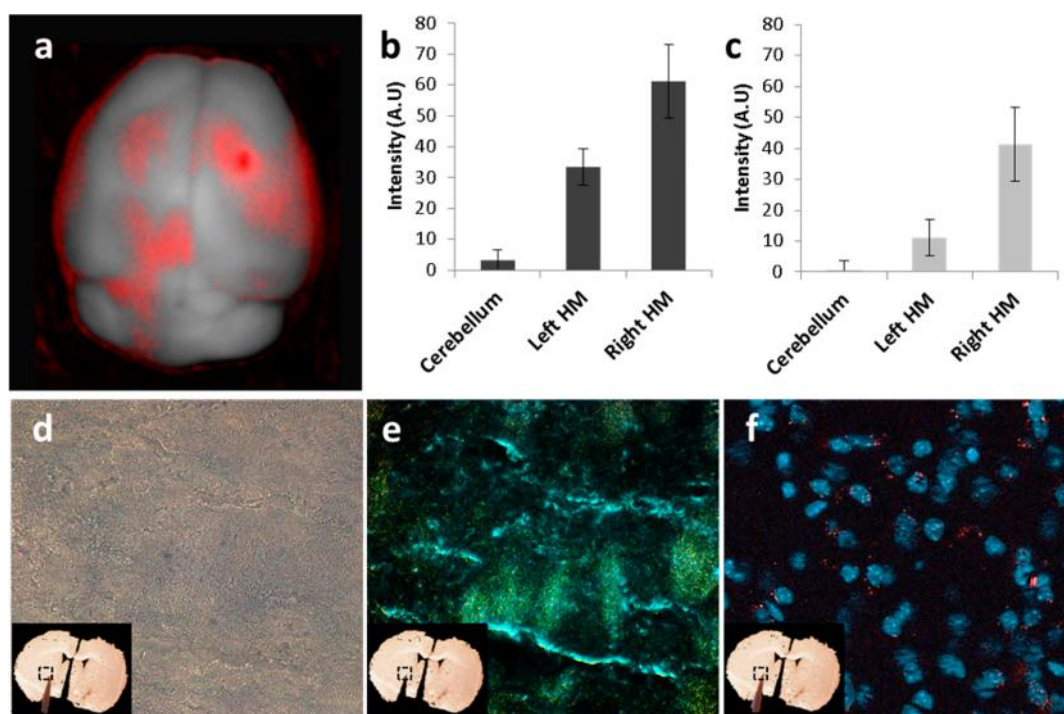


Figure 7. Imaging of double-labeled exosomes. (a) Spectral unmixing image (Maestro) of brain induced with striatal stroke, 24 h post-IN administration of exosomes (red). (b) ImageJ analysis of spectral imaging; color density, translated into intensity, was analyzed in three regions: the cerebellum, the left hemisphere, and the right hemisphere (where the stroke was induced). (c) ImageJ analysis of CT imaging; color density, translated into intensity, was examined in the same three regions as above. (d) Bright-field microscopy of the ischemic striatum (representative section; magnification 40 \times). (e) Dark-field microscopy image of the same section. GNPs are seen in yellow (magnification 40 \times). (f) Histological analysis of the same section, stained with PKH26 (red) and DAPI (blue, for all cells) (magnification 60 \times).

significantly lower compared to the amount of GNPs that were loaded in the exosomes ($p < 0.05$) (Supplementary Figure S6c). These results suggest that the GNPs do not disassociate from the exosomes, but rather remain within them over 24 h.

CT Imaging Correlates with Live Fluorescence Imaging. To establish the proposed exosome labeling protocol as a reliable and consistent imaging technique, we validated the presence of the imaged GNPs within the exosomes 24 h after labeling. This was done using exosomes double-labeled with GNPs and the fluorescent dye PKH26 and comparing *ex vivo* brain CT imaging with spectral unmixing fluorescence imaging.^{61,62}

Focal ischemic-like damage was induced in C57bl/6 male mice ($n = 3$) by a single injection of the vasoconstrictor endothelin-1 into the right striatum. One day later, the mice received IN administration of double-labeled exosomes. *Ex vivo* CT scans and fluorescent imaging of brain were conducted 24 h post-exosome administration. We found that CT imaging correlated well with fluorescence imaging (Pearson's coefficient, $\rho = 0.7$; Figure 7a–c and Supplementary Figure S7b), both showing similar trends of GNP accumulation in the same brain areas. Both imaging modalities showed the highest intensity, indicating the highest amount of GNP accumulation in the ischemic right hemisphere. Additionally, using fluorescent staining and dark-field microscopy, we were able to identify both the exosomes and gold in the same striatal slices (Figure 7d–f and Supplementary Figure S7a). This analysis further verifies that the signal obtained by CT is attributable to the presence of migrated gold-labeled exosomes.

CONCLUSIONS

In the present study, we developed a technique for *in vivo* neuroimaging and tracking of exosomes. We demonstrated that exosomes can be labeled with glucose-coated nanoparticles directly, without the prerequisite of labeling parent cells, and that this labeling occurs *via* an active mechanism that is associated with GLUT-1 glucose transporter. We further found that intranasal administration was more effective than IV injection. The noninvasive IN route confers numerous advantages and is a promising and efficient therapeutic strategy for various CNS diseases. Finally, using CT, we clearly detected accumulation of MSC-derived, GNP-labeled exosomes in the stroke region of the brain, up to 24 h after IN administration, in contrast to the nonlesioned brain. This indicates the homing of MSC-derived exosomes specifically to injured brain regions, and that GNP labeling is crucial for the ability to image and track exosomes *in vivo*. Future research should focus on the mechanism underlying the specific migration of exosomes within the brain in stroke and in other brain pathologies. One of the greatest concerns in longitudinal imaging with nanoparticles is whether they remain internalized within the carrier (in this case, exosomes) after administration or disassociate from the carrier over time. This concern was previously addressed in our *in vitro* and *in vivo* studies on cell tracking.^{9–12} In this study, double-labeling of the exosomes with GNPs and with a fluorescent marker, as well as comparison between brain accumulation patterns of GNP-labeled exosomes and free GNPs, indicated that the GNPs likely remain within the exosomes over 24 h. Nonetheless, there is currently no precise method for ascertaining the presence of GNPs within the exosomes *in vivo* over long periods. Our

method can serve as a general platform for highly sensitive, noninvasive tracking of exosomes within the brain using CT. This approach can significantly promote the study and application of exosome-based therapies for various brain pathologies.

METHODS

Exosome Preparation. Mesenchymal Stem Cell Preparation. Human MSCs were purchased from Lonza (Basel, Switzerland). Cells were cultured and expanded as previously described.⁶³ Prior to exosome collection, the cells were cultured in exosome-free platelets, and 3 days later, the medium was collected.

Exosome Purification Protocol. The exosomes were purified by isolating the culture fluid and centrifuging for 10 min at 300g. The supernatant was recovered and centrifuged for 10 min at 2000g. Once again, the supernatant was recovered and centrifuged for 30 min at 10000g. The supernatant was taken, put through a 0.22 μm filter, and centrifuged for 70 min at 100000g. The pellet, containing the exosomes and proteins, was washed in PBS then centrifuged for 70 min at 100000g. The pellet, containing the purified exosomes, was resuspended in 200 μL of sterilized PBS. Each centrifugation was conducted at 4 $^{\circ}\text{C}$.

Exosome Classification. Nanosight Technology. Nanosight (Merkel Technologies Ltd., Israel) was used to characterize the size and concentration of the exosomes. Western blot for CD9 and calnexin was used to estimate the purification of the sample.

Western Blot. MSC lytat and MSC-exo were solubilized sample buffer (1:4). The samples were preheated at 60 $^{\circ}\text{C}$ for 15 min. SDS/PAGE was carried out on a 4–20% polyacrylamide gel, and proteins were transferred to Immobilon-P membranes (Millipore, Amsterdam, The Netherlands). The membranes were blocked in 5% milk and were probed overnight at 4 $^{\circ}\text{C}$ with CD9 antibody (ABCAM), CD69 (ABCAM), and calnexin (ABCAM) as negative control. After three washes in TBS-Tween 20, membranes were incubated with the secondary antibody (Thermo Scientific, Rockford, IL, USA) for 1 h and washed again. For visualization, blots were exposed to Pierce enhanced chemiluminescent substrate and measured by Uvitec Alliance 2.7 (Cambridge, UK).

GNP Synthesis and Conjugation. 20 nm Synthesis and Conjugation. A total of 0.414 mL of 1.4 M HAuCl_4 solution in 200 mL of water was added to a 250 mL single-neck round-bottom flask. The solution was stirred within an oil bath on a hot plate until it boiled, then 4.04 mL of a 10% sodium citrate solution (0.39 M sodium citrate tribasic dihydrate 98%, Sigma CAS 6132-04-3) was added and stirred for 5 additional minutes. The flask was then removed from the hot oil. To prevent aggregation and stabilize the particles in physiological solutions, PEG7 (95%, Sigma-Aldrich, Israel Ltd.) was absorbed onto the GNPs. First, the solution was centrifuged to dispose of excess citrate. PEG7 solution (2.26×10^3 g) was then added to the GNP solution, and the mixture was stirred overnight and subsequently centrifuged. Next, excess EDC (*N*-ethyl-*N*-(3-(dimethylamino)propyl)carbodiimide (1.87×10^{-3} g) and NHS (*N*-hydroxysuccinimide) (Thermo Fisher Scientific, Inc., Rockford, IL) (2.12×10^3 g) were added to the solution, followed by addition of glucose-2 (2GF) (*D*-(β)-glucosamine hydrochloride, Sigma-Aldrich, Israel Ltd.) (1.75×10^3 g). NHS and EDC form an active ester intermediate with the $-\text{COOH}$ functional groups, which can then undergo an amidation reaction with the glucose NH_2 group. Glucosamine molecule C-2 (2GF-GNP): *D*-(β)-glucosamine hydrochloride (3 mg; Sigma-Aldrich) was added to the activated linker-coated GNPs.

5 nm Synthesis and Conjugation. A mixture of 3.75 mL of oleic acid (65%), linoleic acid (18%), palmitic acid (16%), 15 mL of ethanol, and 200 mg of NaOH were added to 30 mL of DDW. The solution was stirred for 5 min. Fifty milligrams of HAuCl_4 was added while stirring, followed by 5 mL of ascorbic acid (0.05 M), and the solution was stirred for another minute. PEG7 solution (2.26×10^3 g) was then added to the GNP solution, and the mixture was stirred for another hour. The pH was then adjusted to 9 using NaOH, and the solution was stirred for another hour. Eighty milliliters of *n*-hexane was

added, and the solution was stirred for another hour. The pH of the resulting mixture was adjusted to 7 using HCl solution (37%). The mixture was placed in a funnel for phase separation (organic and aqueous). The aqueous phase was evaporated using a vacuum. Next, excess EDC (1.87×10^{-3} g) and NHS (Thermo Fisher Scientific, Inc., Rockford, IL) (2.12×10^3 g) were added to the solution, followed by addition of 2GF (Sigma-Aldrich, Israel Ltd.) (1.75×10^3 g).

GNP Characterization. Transmission electron microscopy (JEM-1400, JEOL) was used to measure the size and shape of the GNPs, which were further characterized using ultraviolet–visible spectroscopy (UV-1650 PC; Shimadzu Corporation, Kyoto, Japan), ζ -potential (ZetaSizer 3000HS; Malvern Instruments, Malvern, UK), and dynamic light scattering.

Gold Quantification with Flame Analysis. Flame atomic absorption spectroscopy (SpectrAA 140, Agilent Technologies) was used to determine amounts of gold in the investigated samples. Exosome samples were dissolved in 30 μL of aqua regia acid (a mixture of nitric acid and hydrochloric acid in a volume ratio of 1:3) and diluted with purified water to a total volume of 4 mL. After filtration of the samples, gold concentrations were determined according to absorbance values, with correlation with calibration curves, constructed from solution with known gold concentrations (0, 2, 5, and 10 mg/L). Body organs (liver, kidney, spleen, lungs, and blood) were melted with 1 mL of aqua regia acid and then evaporated and diluted to a total volume of 4 mL. After filtration of the samples, gold concentrations were determined according to absorbance values, with correlation to calibration curves, constructed from solution with known gold concentrations (0, 2, 5, 10 mg/L). The detection limit of FAAS is 80 ppm.

In Vitro Uptake Mechanism Analysis. Exosomes (total of 2.8×10^{10} , 200 μL exosomes in 1 mL of saline) were incubated at 37 $^{\circ}\text{C}$ for 3 h with glucose-coated GNPs (35 mg/mL, 100 μL) under different conditions. Temperature conditions: incubation with GNPs at 4 or 37 $^{\circ}\text{C}$. Enriched glucose environment: 10 mg of *D*-glucose (Sigma-Aldrich, Israel) added to the exosomes + saline solution for 20 min followed by incubation with GNPs (37 $^{\circ}\text{C}$). Glucose inhibitor: 60 μL of glucose inhibitor cytochalasin B (Abcam, Israel) (5 mg/mL) added to the exosomes + saline solution for 20 min followed by incubation with GNPs (37 $^{\circ}\text{C}$). Nonspecific serine endopeptidase: 7 μL of proteinase-K (Roche Diagnostics, Germany) added to the exosomes + saline solution for 10 min at 55 $^{\circ}\text{C}$ while shaking, followed by 7 μL inhibitor (phenylmethanesulfonyl fluoride, Sigma-Aldrich, Israel) (10 mg/mL) for 10 min, followed by incubation with GNPs (37 $^{\circ}\text{C}$, 3 h). After the incubation with GNPs, the exosomes were centrifuged for 2 h (100000g, 4 $^{\circ}\text{C}$); the exosome pellet was collected, and the amount of gold was determined using FAAS analysis.

Animal Care. All animals were maintained on a 12/12 h light/dark cycle under fixed conditions of temperature (23 $^{\circ}\text{C}$) and humidity (50%), with free access to food and water. All experimental procedures and methods were approved by the Animal Care Committee of Bar-Ilan University and performed in accordance with the National Institutes of Health guidelines and regulations.

Administration of Exosomes. C57bl/6 male mice ($n = 3$ in each test group (IV/IN/control)) were bred from adult pairs originally purchased from Jackson Laboratory (Bar Harbor, ME). Mice were housed in groups of 3–5 littermates per cage. At 5 weeks of age, mice were given exosomes by intranasal or intravenous administrations. For IN administrations, 2.8×10^9 exosomes, total volume of 20 μL , were administered slowly, 2.5 μL each dose. For IV administration, the same amount of exosomes (2.8×10^9) with total volume of 150 μL were injected slowly into the tail vein.

Stroke Model. C57bl/6 male mice, $n = 3$ for each test group (stroke/control/double staining) and for each time point (1 h/3 h/24 h), received stereotactic injection of 2 μL of endothelin-1 or saline into the right striatum (coordinates: anterior +0.5, lateral +1.9, ventral -2.9 mm from bregma). One day later, mice received exosomes (2.8×10^9) by intranasal administration.

CT Imaging. In Vivo Scans. of the brains were performed using a micro-CT scanner (Bruker, Skyscan high-resolution model 1176) with a nominal resolution of 35 μm , a 0.2 mm aluminum filter, and a tube

voltage of 45 kV. Reconstruction was done with a modified Feldkamp algorithm⁶⁴ using the SkyScanNRecon software accelerated by GPU. Ring artifact reduction, Gaussian smoothing (3%), and beam hardening correction (25%) were applied. Volume rendered 3D images were generated using an RGBA transfer function in SkyScan CT-Volume (“CT-Vol”) and CT-Voxel (“CT-Vox”) software.

Ex Vivo Scans. Additional nonionic iodinated contrast agent (lopamidol, Bayer Schering Pharma, Japan) was used in order to differentiate between different brain tissue types. Brains were removed and placed in 10% buffered formalin for 3 days of fixation, then soaked in lopamidol (150 mg/mL) diluted with 7.5% paraformaldehyde at 4 °C for 7 days. Prior to CT imaging, brains were removed from the solution, blotted dry, and placed in a sample holder for imaging. The sample holder was sealed with plastic film to prevent dehydration. Brains were then scanned in the micro-CT at a nominal resolution (pixel size) of 18 μm, employing an aluminum filter 0.2 mm thick and an applied X-ray tube voltage of 45 kV. The scan orbit was 180 with a rotation step of 0.5. Reconstruction was carried out using the NRecon software accelerated by GPU. Gaussian smoothing (3%), ring artifact reduction, and beam hardening correction (25%) were applied. The cross-section slices were stored in 8-bit BMP format (256 shades of gray).

Ex Vivo Gold Quantification. Inductively coupled plasma spectrometry (ICP-OES 710, Agilent Technologies) was used to determine amounts of gold in the investigated samples. Brain tissues were melted with 1 mL of aqua regia acid and then evaporated and diluted to a total volume of 4 mL. After filtration of the samples, gold concentrations were determined according to absorbance values, with correlation to calibration curves, constructed from solution with known gold concentrations (0, 0.5, 2, and 5 mg/L). The detection limit of ICP is 50 ppb.

Spectral Unmixing Imaging. Exosome Staining with pKH. Stock solution was created by mixing 2 μL of pKH26 in 500 μL of diluent. From the stock, 100 μL was added to 50 μL of exosomes in PBS. After 5 min, 100 μL of exosome-free platelets was added to the previous mixture and then centrifuged for 90 min at 100g at 4 °C. The pellet was suspended in 200 μL of PBS.

Imaging Preparation. Mice aged 6–7 weeks were administered 20 μL labeled exosomes intranasally (two doses of 5 μL in each nostril alternatively). Twenty-four hours post-administration mice were sacrificed by perfusion of PBS and post-fixation of 4% PFA. The brains were incubated at 4 °C for 24 h in 4% PFA, followed by 24 h in 30% sucrose and then moved to PBS 0.4% sodium azide. Whole brain fluorescence imaging was obtained using spectral unmixing fluorescence imaging (CRL, Maestro, UT Southwestern, USA) excitation filter of 523 nm and emission filter of 560 nm. Superposition of distribution patterns was composed using ImageJ software (1.48 V, National Institutes of Health, USA).

Immunostaining. Exosomes labeling (prior to intranasal administration): 5 μL of (Sigma-Aldrich) were suspended in PBS with 200 μL exosomes for 5 min, followed by 10 min of ultracentrifuge. The exosomes pellet was then resuspended in PBS. Animals under deep anesthesia were transcardially perfused with 1× PBS followed by 4% paraformaldehyde. Excised brains were postfixed in paraformaldehyde (24 h, 4 °C), then equilibrated in PBS containing 30% sucrose (48 h, 4 °C), and gradually frozen in dry ice. Tissues were cryosectioned (10 μm) in the coronal plane. Representative brain slices were washed in PBS, blocked with a blocking solution for 1 h, and then stained with DAPI (1:1000, Abcam) for 5 min and washed in PBS. Fluorescent images were acquired with an ApoTome microscope.

Image Analysis. An image analysis program (ImageJ) was used to transform the images obtained from the different modalities (CT and Maestro) to have the same range of colors, on an RGB 8-bit scale. Color density was measured in three regions (the same area size was measured in each): the cerebellum, left hemisphere, and right hemisphere.

Statistical Analysis. All experiments were repeated three times, and each experiment had at least $n = 3$ measurements. Differences between two groups were analyzed using Student's t test. One-way ANOVA was performed for comparing more than two groups. Based

on the image analysis, correlation was calculated using Pearson's coefficient correlation.

ASSOCIATED CONTENT

Supporting Information

The Supporting Information is available free of charge on the ACS Publications website at DOI: 10.1021/acsnano.7b04495.

Supplementary Figures S1–S7(PDF)

AUTHOR INFORMATION

Corresponding Author

*Phone: +972-3-5317509 (office); +972-3-5314647 (lab). E-mail: rachel.popovtzer@biu.ac.il.

ORCID

Oshra Betzer: 0000-0002-4429-7024

Author Contributions

[†]O.B. and N.P. contributed equally to the work.

Notes

The authors declare no competing financial interest.

ACKNOWLEDGMENTS

We thank Dr. A. Ayoub for her help in preparing and characterizing 5 nm GNPs. This work was partially supported by the Ministry of Science, Technology & Space doctoral scholarship for O.B.

REFERENCES

- (1) Van Niel, G.; Porto-Carreiro, I.; Simoes, S.; Raposo, G. Exosomes: A Common Pathway for a Specialized Function. *J. Biochem.* **2006**, *140*, 13–21.
- (2) Chai, R.; Wee, R.; Yeo, Y.; Hian, K.; Kiang, S. Exosomes for Drug Delivery — a Novel Application for the Mesenchymal Stem Cell. *Biotechnol. Adv.* **2013**, *31*, 543–551.
- (3) Haney, M. J.; Klyachko, N. L.; Zhao, Y.; Gupta, R.; Plotnikova, E. G.; He, Z.; Patel, T.; Piroyan, A.; Sokolsky, M.; Kabanov, A. V.; et al. Exosomes as Drug Delivery Vehicles for Parkinson's Disease Therapy. *J. Controlled Release* **2015**, *207*, 18–30.
- (4) Liu, Y.; Li, D.; Liu, Z.; Zhou, Y.; Chu, D.; Li, X.; Jiang, X.; Hou, D.; Chen, X.; Chen, Y.; et al. Targeted Exosome-Mediated Delivery of Opioid Receptor Mu siRNA for the Treatment of Morphine Relapse. *Sci. Rep.* **2015**, *5*, 17543.
- (5) Johnsen, K. B.; Gudbergsson, J. M.; Skov, M. N.; Pilgaard, L.; Moos, T.; Duroux, M. A Comprehensive Overview of Exosomes as Drug Delivery Vehicles - Endogenous Nanocarriers for Targeted Cancer Therapy. *Biochim. Biophys. Acta, Rev. Cancer* **2014**, *1846*, 75–87.
- (6) Sun, D.; Zhuang, X.; Xiang, X.; Liu, Y.; Zhang, S.; Liu, C.; Barnes, S.; Grizzle, W.; Miller, D.; Zhang, H.-G. A Novel Nanoparticle Drug Delivery System: The Anti-Inflammatory Activity of Curcumin Is Enhanced When Encapsulated in Exosomes. *Mol. Ther.* **2010**, *18*, 1606–1614.
- (7) Yuan, D.; Zhao, Y.; Banks, W. A.; Bullock, K. M.; Haney, M.; Batrakova, E.; Kabanov, A. V. Macrophage Exosomes as Natural Nanocarriers for Protein Delivery to Inflamed Brain. *Biomaterials* **2017**, *142*, 1–12.
- (8) Yu, B.; Zhang, X.; Li, X. Exosomes Derived from Mesenchymal Stem Cells. *Int. J. Mol. Sci.* **2014**, *15*, 4142–4157.
- (9) Lai, R. C.; Yeo, R. W. Y.; Tan, K. H.; Lim, S. K. Exosomes for Drug Delivery - A Novel Application for the Mesenchymal Stem Cell. *Biotechnol. Adv.* **2013**, *31*, 543–551.
- (10) Betzer, O.; Schwartz, A.; Motiei, M.; Kazimirsky, G.; Gispán, I.; Danti, E.; Brodie, C.; Yadid, G.; Popovtzer, R. Nanoparticle-Based CT Imaging Technique for Longitudinal and Quantitative Stem Cell Tracking within the Brain: Application in Neuropsychiatric Disorders. *ACS Nano* **2014**, *8*, 9274–9285.

- (11) Janowski, M.; Bulte, J. W. M.; Walczak, P. Personalized Nanomedicine Advancements for Stem Cell Tracking. *Adv. Drug Delivery Rev.* **2012**, *64*, 1488–1507.
- (12) Sun, D.; Zhuang, X.; Xiang, X.; Liu, Y.; Zhang, S.; Liu, C.; Barnes, S.; Grizzle, W.; Miller, D.; Zhang, H.-G. A Novel Nanoparticle Drug Delivery System: The Anti-Inflammatory Activity of Curcumin Is Enhanced When Encapsulated in Exosomes. *Mol. Ther.* **2010**, *18*, 1606–1614.
- (13) Shwartz, A.; Betzer, O.; Kronfeld, N.; Kazimirsky, G.; Cazacu, S.; Finniss, S.; Kyung Lee, H.; Motiei, M.; Yael Dagan, S.; Popovtzer, R.; et al. Therapeutic Effect of Astroglia-like Mesenchymal Stem Cells Expressing Glutamate Transporter in a Genetic Rat Model of Depression. *Theranostics* **2017**, *7*, 2690–2703.
- (14) Zhuang, X.; Xiang, X.; Grizzle, W.; Sun, D.; Zhang, S.; Axtell, R. C.; Ju, S.; Mu, J.; Zhang, L.; Steinman, L.; et al. Treatment of Brain Inflammatory Diseases by Delivering Exosome Encapsulated Anti-Inflammatory Drugs From the Nasal Region to the Brain. *Mol. Ther.* **2011**, *19*, 1769–1779.
- (15) Yang, T.; Martin, P.; Fogarty, B.; Brown, A.; Schurman, K.; Phipps, R.; Yin, V. P.; Lockman, P.; Bai, S. Exosome Delivered Anticancer Drugs across the Blood-Brain Barrier for Brain Cancer Therapy in Danio Rerio. *Pharm. Res.* **2015**, *32*, 2003–2014.
- (16) Ali, I. U.; Chen, X. Penetrating the Blood-Brain Barrier: Promise of Novel Nanoplatfoms and Delivery Vehicles. *ACS Nano* **2015**, *9*, 9470–9474.
- (17) Haney, M. J.; Klyachko, N. L.; Zhao, Y.; Gupta, R.; Plotnikova, E. G.; He, Z.; Patel, T.; Piroyan, A.; Sokolsky, M.; Kabanov, A. V.; et al. Exosomes as Drug Delivery Vehicles for Parkinson's Disease Therapy. *J. Controlled Release* **2015**, *207*, 18–30.
- (18) Zilony, N.; Tzur-Balter, A.; Segal, E.; Shefi, O. Bombarding Cancer: Biolistic Delivery of Therapeutics Using Porous Si Carriers. *Sci. Rep.* **2013**, *3*, 2499.
- (19) Takahashi, Y.; Nishikawa, M.; Shinotsuka, H.; Matsui, Y.; Ohara, S.; Imai, T.; Takakura, Y. Visualization and *in Vivo* Tracking of the Exosomes of Murine Melanoma B16-BL6 Cells in Mice after Intravenous Injection. *J. Biotechnol.* **2013**, *165*, 77–84.
- (20) Marzola, P.; Busato, A.; Bonafede, R.; Bontempi, P.; Scambi, I.; Schiaffino, L.; Benati, D.; Malatesta, M.; Sbarbati, A.; Mariotti, R. Magnetic Resonance Imaging of Ultrasmall Superparamagnetic Iron Oxide-Labeled Exosomes from Stem Cells: A New Method to Obtain Labeled Exosomes. *Int. J. Nanomed.* **2016**, *11*, 2481–2490.
- (21) Yang, T.; Martin, P.; Fogarty, B.; Brown, A.; Schurman, K.; Phipps, R.; Yin, V. P.; Lockman, P.; Bai, S. Exosome Delivered Anticancer Drugs across the Blood-Brain Barrier for Brain Cancer Therapy in Danio Rerio. *Pharm. Res.* **2015**, *32*, 2003–2014.
- (22) Pasternak, O.; Kubicki, M.; Shenton, M. E. *In Vivo* Imaging of Neuroinflammation in Schizophrenia. *Schizophr. Res.* **2016**, *173*, 200–212.
- (23) Horton, N. Three-Photon Microscopy At 1700 Nm For *In Vivo* Imaging. Ph.D Thesis, Cornell University, 2015.
- (24) Betzer, O.; Meir, R.; Dreifuss, T.; Shamalov, K.; Motiei, M.; Shwartz, A.; Baranes, K.; Cohen, C. J.; Shraga-Heled, N.; Ofir, R.; et al. *In-Vitro* Optimization of Nanoparticle-Cell Labeling Protocols for *In-Vivo* Cell Tracking Applications. *Sci. Rep.* **2015**, *5*, 15400.
- (25) Meir, R.; Betzer, O.; Motiei, M.; Kronfeld, N.; Brodie, C.; Popovtzer, R. Design Principles for Noninvasive, Longitudinal and Quantitative Cell Tracking with Nanoparticle-Based CT Imaging. *Nanomedicine* **2017**, *13*, 421–429.
- (26) Dreifuss, T.; Betzer, O.; Shilo, M.; Popovtzer, A.; Motiei, M.; Popovtzer, R. A Challenge for Theranostics: Is the Optimal Particle for Therapy Also Optimal for Diagnostics? *Nanoscale* **2015**, *7*, 15175.
- (27) Meir, R.; Shamalov, K.; Betzer, O.; Motiei, M.; Horovitz-Fried, M.; Yehuda, R.; Popovtzer, A.; Popovtzer, R.; Cohen, C. J. Nanomedicine for Cancer Immunotherapy: Tracking Cancer-Specific T-Cells *in Vivo* with Gold Nanoparticles and CT Imaging. *ACS Nano* **2015**, *9*, 6363–6372.
- (28) Popovtzer, A.; Mizrachi, A.; Motiei, M.; Bragilovski, D.; Lubimov, L.; Levi, M.; Hilly, O.; Ben-Aharon, I.; Popovtzer, R. Actively Targeted Gold Nanoparticles as Novel Radiosensitizer Agents: An *in Vivo* Head and Neck Cancer Model. *Nanoscale* **2016**, *8*, 2678–2685.
- (29) Betzer, O.; Ankri, R.; Motiei, M.; Popovtzer, R. Theranostic Approach for Cancer Treatment: Multifunctional Gold Nanorods for Optical Imaging and Photothermal Therapy. *J. Nanomater.* **2015**, *2015*, 646713.
- (30) Arvizo, R.; Bhattacharya, R.; Mukherjee, P. Gold Nanoparticles: Opportunities and Challenges in Nanomedicine. *Expert Opin. Drug Delivery* **2010**, *7*, 753–763.
- (31) Reuveni, T.; Motiei, M.; Romman, Z.; Popovtzer, A.; Popovtzer, R. Targeted Gold Nanoparticles Enable Molecular CT Imaging of Cancer: An *in Vivo* Study. *Int. J. Nanomed.* **2011**, *6*, 2859–2864.
- (32) Betzer, O.; Meir, R.; Motiei, M.; Yadid, G.; Popovtzer, R. Gold Nanoparticle-Cell Labeling Methodology for Tracking Stem Cells within the Brain. *Proc. SPIE* **2017**, 100771F.
- (33) Alhasan, A. H.; Patel, P. C.; Choi, C. H. J.; Mirkin, C. A. Exosome Encased Spherical Nucleic Acid Gold Nanoparticle Conjugates as Potent microRNA Regulation Agents. *Small* **2014**, *10*, 186–192.
- (34) Roma-Rodrigues, C.; Pereira, F.; Alves de Matos, A. P.; Fernandes, M.; Baptista, P. V.; Fernandes, A. R. Smuggling Gold Nanoparticles across Cell Types – a New Role for Exosomes in Gene Silencing. *Nanomedicine* **2017**, *13*, 1389–1398.
- (35) Mahmood, A.; Lu, D.; Chopp, M. Intravenous Administration of Marrow Stromal Cells (MSCs) Increases the Expression of Growth Factors in Rat Brain after Traumatic Brain Injury. *J. Neurotrauma* **2004**, *21*, 33–39.
- (36) Budnik, V.; Ruiz-Cañada, C.; Wendler, F. Extracellular Vesicles Round off Communication in the Nervous System. *Nat. Rev. Neurosci.* **2016**, *17*, 160–172.
- (37) Xin, H.; Li, Y.; Cui, Y.; Yang, J. J.; Zhang, Z. G.; Chopp, M. Systemic Administration of Exosomes Released from Mesenchymal Stromal Cells Promote Functional Recovery and Neurovascular Plasticity after Stroke in Rats. *J. Cereb. Blood Flow Metab.* **2013**, *33*, 1711–1715.
- (38) Dreifuss, T.; Betzer, O.; Shilo, M.; Popovtzer, A.; Motiei, M.; Popovtzer, R. A Challenge for Theranostics: Is the Optimal Particle for Therapy Also Optimal for Diagnostics? *Nanoscale* **2015**, *7*, 15175.
- (39) Segal-Gavish, H.; Karvat, G.; Barak, N.; Barzilay, R.; Ganz, J.; Edry, L.; Aharony, I.; Offen, D.; Kimchi, T. Mesenchymal Stem Cell Transplantation Promotes Neurogenesis and Ameliorates Autism Related Behaviors in BTBR Mice. *Autism Res.* **2016**, *9*, 17–32.
- (40) Munson, P.; Shukla, A. Exosomes: Potential in Cancer Diagnosis and Therapy. *Medicines* **2015**, *2*, 310–327.
- (41) Vader, P.; Mol, E. A.; Pasterkamp, G. Extracellular Vesicles for Drug Delivery. *Adv. Drug Delivery Rev.* **2016**, *106*, 148–156.
- (42) Brites, D.; Fernandes, A. Neuroinflammation and Depression: Microglia Activation, Extracellular Microvesicles and microRNA Dysregulation. *Front. Cell. Neurosci.* **2015**, *9*, 476.
- (43) Betzer, O.; Shilo, M.; Opochinsky, R.; Barnoy, E.; Motiei, M.; Okun, E.; Yadid, G.; Popovtzer, R. The Effect of Nanoparticle Size on the Ability to Cross the Blood-brain Barrier: An *in Vivo* Study. *Nanomedicine (London, U. K.)* **2017**, *12*, 1533.
- (44) Mulcahy, L. A.; Pink, R. C.; Carter, D. R. F. Routes and Mechanisms of Extracellular Vesicle Uptake. *J. Extracell. Vesicles* **2014**, *3*, 24641.
- (45) Drin, G.; Cottin, S.; Blanc, E.; Rees, A. R.; Temsamani, J. Studies on the Internalization Mechanism of Cationic Cell-Penetrating Peptides. *J. Biol. Chem.* **2003**, *278*, 31192–31201.
- (46) Mironava, T.; Hadjiargyrou, M.; Simon, M.; Jurukovski, V.; Rafailovich, M. H. Gold Nanoparticles Cellular Toxicity and Recovery: Effect of Size, Concentration and Exposure Time. *Nanotoxicology* **2010**, *4*, 120–137.
- (47) Zhang, Q.; Li, X.; Zhang, Q. Cellular Uptake Mechanism and Intracellular Fate of Hydrophobically Modified Pullulan Nanoparticles. *Int. J. Nanomed.* **2013**, *8*, 1825–1834.
- (48) Gheczy, N.; Kuchler, A.; Walde, P. Proteinase K Activity Determination with Beta-Galactosidase as Sensitive Macromolecular Substrate. *Anal. Biochem.* **2016**, *513*, 54–60.

- (49) RS, B.; Leung, J.; Kison, P.; Zasadny, K.; Flint, A.; Wahl, R. Glucose Transporters and FDG Uptake in Untreated Primary Human Non-Small Cell Lung Cancer. *J. Nucl. Med.* **1999**, *40*, 556–565.
- (50) Motiei, M.; Dreifuss, T.; Betzer, O.; Panet, H.; Popovtzer, A.; Santana, J.; Abourbeh, G.; Mishani, E.; Popovtzer, R. Differentiating Between Cancer and Inflammation: A Metabolic-Based Method for Functional Computed Tomography Imaging. *ACS Nano* **2016**, *10*, 3469.
- (51) Garcia, N. A.; Moncayo-Arlandi, J.; Sepulveda, P.; Diez-Juan, A. Cardiomyocyte Exosomes Regulate Glycolytic Flux in Endothelium by Direct Transfer of GLUT Transporters and Glycolytic Enzymes. *Cardiovasc. Res.* **2016**, *109*, 397–408.
- (52) Fong, M. Y.; Zhou, W.; Liu, L.; Alontaga, A. Y.; Chandra, M.; Ashby, J.; Chow, A.; O'Connor, S. T.; Li, S.; Chin, A. R.; et al. Breast-Cancer-Secreted miR-122 Reprograms Glucose Metabolism in Premetastatic Niche to Promote Metastasis. *Nat. Cell Biol.* **2015**, *17*, 183–194.
- (53) Pinkofsky, H. B.; Dwyer, D. S.; Bradley, R. J. The Inhibition of GLUT1 Glucose Transport and Cytochalasin B Binding Activity by Tricyclic Antidepressants. *Life Sci.* **1999**, *66*, 271–278.
- (54) Paslakis, G.; Blum, W. F.; Deuschle, M. Intranasal Insulin-like Growth Factor I (IGF-I) as a Plausible Future Treatment of Depression. *Med. Hypotheses* **2012**, *79*, 222–225.
- (55) Pires, A.; Fortuna, A.; Alves, G.; Falcão, A. Intranasal Drug Delivery: How, Why and What For? *J. Pharm. Pharm. Sci.* **2009**, *12*, 288–311.
- (56) van Woensel, M.; Wauthoz, N.; Rosière, R.; Amighi, K.; Mathieu, V.; Lefranc, F.; van Gool, S. W.; de Vleeschouwer, S. Formulations for Intranasal Delivery of Pharmacological Agents to Combat Brain Disease: A New Opportunity to Tackle GBM? *Cancers* **2013**, *5*, 1020–1048.
- (57) Wiklander, O. P. B.; Nordin, J. Z.; O'Loughlin, A.; Gustafsson, Y.; Corso, G.; Mäger, I.; Vader, P.; Lee, Y.; Sork, H.; Seow, Y.; et al. Extracellular Vesicle *in Vivo* Biodistribution Is Determined by Cell Source, Route of Administration and Targeting. *J. Extracell. Vesicles* **2015**, *4*, 26316.
- (58) Martin, J.-R. *In Vivo* Brain Imaging: Fluorescence or Bioluminescence, Which to Choose? *J. Neurogenet.* **2008**, *22*, 285–307.
- (59) Danielyan, L.; Schäfer, R.; von Ameln-Mayerhofer, A.; Bernhard, F.; Verleysdonk, S.; Buadze, M.; Lourhmati, A.; Klopfer, T.; Schaumann, F.; Schmid, B.; et al. Therapeutic Efficacy of Intranasally Delivered Mesenchymal Stem Cells in a Rat Model of Parkinson Disease. *Rejuvenation Res.* **2011**, *14*, 3–16.
- (60) Kordelas, L.; Rebmann, V.; Ludwig, A.-K.; Radtke, S.; Ruesing, J.; Doeppner, T. R.; Epple, M.; Horn, P. A.; Beelen, D. W.; Giebel, B. MSC-Derived Exosomes: A Novel Tool to Treat Therapy-Refractory Graft-versus-Host Disease. *Leukemia* **2014**, 970–974.
- (61) Fixler, D.; Nayhoz, T.; Ray, K. Diffusion Reflection and Fluorescence Lifetime Imaging Microscopy Study of Fluorophore-Conjugated Gold Nanoparticles or Nanorods in Solid Phantoms. *ACS Photonics* **2014**, *1*, 900–905.
- (62) Fixler, D.; Garcia, J.; Zalevsky, Z.; Weiss, A.; Deutsch, M. Speckle Random Coding for 2D Super Resolving Fluorescent Microscopic Imaging. *Micron* **2007**, *38*, 121–128.
- (63) Théry, C.; Amigorena, S.; Raposo, G.; Clayton, A. Isolation and Characterization of Exosomes from Cell Culture Supernatants. *Current Protocols in Cell Biology*; John Wiley & Sons: Hoboken, NJ, 2006; Vol. 3, pp 1–29.
- (64) Feldkamp, L. A.; Davis, L. C.; Kress, J. W. Practical Cone-Beam Algorithm. *J. Opt. Soc. Am. A* **1984**, *1*, 612.